



**HAL**  
open science

## Hydroconversion of 5-Hydroxymethylfurfural to 2,5-Dimethylfuran and 2,5-Dimethyltetrahydrofuran over Non-promoted Ni/SBA-15

Shuo Chen, Carmen Ciotonea, Karine de Oliveira Vigier, François Jérôme, Robert Wojcieszak, Franck Dumeignil, Eric Marceau, Sébastien Royer

► **To cite this version:**

Shuo Chen, Carmen Ciotonea, Karine de Oliveira Vigier, François Jérôme, Robert Wojcieszak, et al.. Hydroconversion of 5-Hydroxymethylfurfural to 2,5-Dimethylfuran and 2,5-Dimethyltetrahydrofuran over Non-promoted Ni/SBA-15. *ChemCatChem*, 2020, 12 (7), pp.2050-2059. 10.1002/cctc.201902028 . hal-02906610

**HAL Id: hal-02906610**

**<https://hal.science/hal-02906610v1>**

Submitted on 19 Nov 2020

**HAL** is a multi-disciplinary open access archive for the deposit and dissemination of scientific research documents, whether they are published or not. The documents may come from teaching and research institutions in France or abroad, or from public or private research centers.

L'archive ouverte pluridisciplinaire **HAL**, est destinée au dépôt et à la diffusion de documents scientifiques de niveau recherche, publiés ou non, émanant des établissements d'enseignement et de recherche français ou étrangers, des laboratoires publics ou privés.

# Hydrogenation of 5-hydroxymethylfurfural to 2,5-dimethylfuran and 2,5-dihydroxymethyltetrahydrofuran over Ni/SBA-15

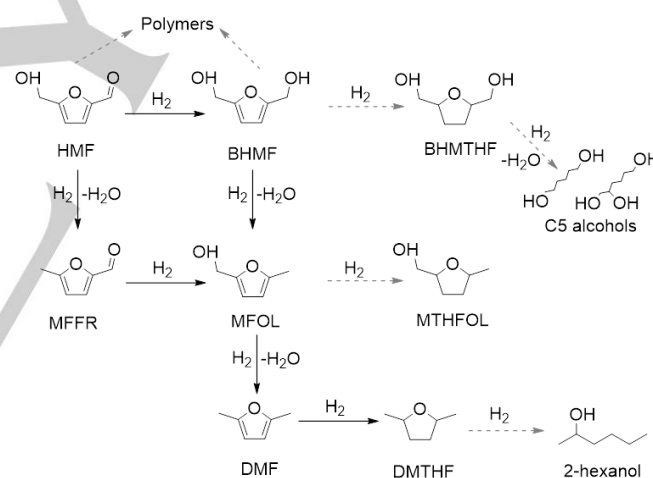
Shuo Chen,<sup>[a]</sup> Carmen Ciotonea,<sup>[a]</sup> Karine De Oliveira Vigier,<sup>[b]</sup> François Jérôme,<sup>[b]</sup> Robert Wojcieszak,<sup>[a]</sup> Franck Dumeignil,<sup>[a]</sup> Eric Marceau,<sup>[a]</sup> Sebastien Royer\*<sup>[a]</sup>

**Abstract:** Selective hydroconversion of 5-hydroxymethylfurfural (HMF) is of great importance for future chemical and energy supply. Herein, we demonstrate that a monometallic Ni/SBA-15 catalyst, prepared by simple Incipient Wetness Impregnation (IWI) using nickel nitrate precursor, can selectively convert HMF to 2,5-dimethylfuran (DMF) or to 2,5-dimethyltetrahydrofuran (DMTHF) under optimized reaction conditions. The mesopore confined Ni particles facilitate the hydrogenolysis and furan ring hydrogenation reactions. Through the control over reaction time, high yields to DMF (71%, at conversion of 93%) and to DMTHF (97%, at conversion of 100%) can be achieved. The kinetic study affords the determination of a preferential reaction route from HMF to DMTHF through 5-methylfurfural (MFFR) formation as intermediate. Favored route then involves the hydrogenolysis of the hydroxyl group as first step (MFFR production), followed by aldehyde function hydrogenation step to methylfurfuryl alcohol (MFOL).

## Introduction

The selective production of biofuels with high octane numbers and energy densities, such as 2,5-dimethylfuran (DMF) and 2,5-dimethyltetrahydrofuran (DMTHF) is currently highly sought for. These two molecules derive from 5-hydroxymethylfurfural (HMF), a platform molecules produced by dehydration of hexoses [1]. HMF contains a furan ring bearing both a pending aldehyde function at the C2-position, and a hydroxymethyl group at the C5-position [2]. The transformation of HMF to DMF may go through two routes, both involving the hydrogenolysis of the side-groups, either starting with the hydrogenation reaction of the aldehyde function, giving 2,5-bis(hydroxymethyl)furan (BHMF) as an intermediate product, or with the hydrogenolysis of the hydroxyl group, giving 5-methylfurfural (MFFR) as an intermediate product (Scheme 1) [3–6]. The formation of DMTHF is usually supposed to take place via the furan ring hydrogenation of DMF, rather than from the hydrogenolysis of hydroxymethyl tetrahydrofurans [7]. Competing polymerization and ring opening reactions may also occur.

HMF being a multifunctional compound, one challenge in its upgrading is to increase the selectivity to the valuable products, as undesired reactions can readily occur in this network of parallel and consecutive reactions. Catalysts based on noble metals such as Pt, Pd, and Ru have proved to be highly active and selective in the reductive transformation of HMF to DMF and DMTHF. For the production of DMF, a CuRu/C catalyst was first explored giving a yield of 76–79% [8]. The best performance was obtained with a Pd/C catalyst under supercritical conditions, achieving a total conversion of HMF to DMF in water at 80 °C, under 10 MPa CO<sub>2</sub> and 1 MPa H<sub>2</sub> after 2 h. For the synthesis of DMTHF, a sulfur-modified Pt/C catalyst was firstly proposed with a yield of 50% [9]. However, noble metal-based catalysts suffer from the limited availability and high cost of the metals, which may hinder their commercial applications on a large scale [10–15].



**Scheme 1.** Hydrogenation of HMF to DMF and DMTHF and possible side reactions (dotted arrows represent side reactions).

Substitutes should be found in non-noble transition metals (e.g., Cu, Co or Ni), which are more abundant but generally less active. High yields of DMF and/or DMTHF generally require bimetallic combinations (Ni-Cu, Ni-Fe, Cu-Co, Cu-Zn, etc.), bifunctional catalysts containing both metallic and acidic active sites, and/or the use of supports that participate in the reaction via their specific surface properties (TiO<sub>2</sub>, ZnO) [16–28]. For example, Seemala et al. used TiO<sub>2</sub> as support to selectively form strong Ni-TiO<sub>2</sub> interactions in Cu-Ni/TiO<sub>2</sub>, which resulted in a deficit of Ni at the particle surface and a promotion of Cu hydrogenation activity without compromising selectivity [20]. As a result, Cu-Ni/TiO<sub>2</sub> gave a DMF yield of 84% at complete conversion at 200 °C under 2.5 MPa in 1,4-dioxane after 8 h. Luo et al. showed that bimetallic

[a] Dr. Shuo Chen, Dr. Carmen Ciotonea, Dr. Robert Wojcieszak, Dr. Eric Marceau, Prof. Sebastien Royer  
Univ. Lille, CNRS, Centrale Lille, ENSCL, Univ. Artois, UMR 8181 - UCCS - Unité de Catalyse et Chimie du Solide, F-59000 Lille, France

E-mail: sebastien.royer@univ-lille.fr

[b] Prof. Karine Vigier De Oliveira  
IC2MP – UMR CNRS 7285, University de Poitiers, F-86000 Poitiers, France

carbon-supported NiCu<sub>3</sub> nanocrystals prepared by a solvothermal method, and consisting of a Cu-rich core and a 1:1 molar Ni:Cu shell, led to an excellent DMF yield of 99% at complete conversion at 180 °C under 3.3 MPa in a continuous flow reactor [23].

Since an emphasis was put early on the need for an auxiliary metal or for surface acidic sites to obtain a selective catalyst, the catalytic properties of monometallic catalysts based on non-noble metals have been paradoxically less explored [29–31]. Ni-based catalysts are known for their hydrogenation ability [32], but successes in the selective conversion of HMF have mostly been achieved with multifunctional catalysts, e.g. Ni-W<sub>2</sub>C/C, Ni-Fe/CNTs (carbon nanotubes), Ni/LaFeO<sub>3</sub> and others [24,26,27,33].

Kong et al. have published a series of papers [25, 28, 31–32] in which the reactivity of monometallic Ni catalysts was investigated. Raney Ni was shown to be active in the hydrogenation of the aldehyde function and of the furan ring of HMF to BHMTFH at 100 °C in dioxane, while the hydrogenation and hydrogenolysis of the side-groups to DMF was favored at a higher temperature, 180 °C [31]. The hydrogenation of the furan ring was not as predominant at 180 °C as it was at 100 °C, with DMTHF building only slowly from DMF at that temperature. It was concluded by the authors that the methyl groups of DMF inhibited its adsorption on the Ni surface. The presence of acidic groups on the catalyst surface was considered as critical to promote both hydrogenolysis reactions and the hydrogenation of the furan ring on Ni. In later works by the same team [28]. Lewis acidic sites were formed through the incomplete reduction of Ni<sup>2+</sup> ions from a phyllosilicate precursor, or from an aluminic support derived from the decomposition of a hydrotalcite. The production of DMTHF was almost quantitative at 150 °C in the first case, and at 180 °C in the second case. In contrast, the hydrogenolysis properties of 20 and 36 Ni wt% catalysts supported on silica, a support that lacks of acidic groups, and prepared by impregnation, were quite poor, even at 180 °C, and a wide slate of products was obtained. Finally, DMF and DMTHF were observed to be formed in a parallel manner on the hydrotalcite-derived catalyst at 180 °C, and not consecutively as would be expected, and as was found on Raney Ni [28,32].

In the present paper, we propose to re-examine the catalytic properties of the monometallic Ni/SiO<sub>2</sub> system, by using a Ni/SBA-15 catalyst prepared following the incipient wetness impregnation – mild drying method (IWI-MD), the SBA-15 support being chosen for its high surface area. Reaction conditions were screened for the production of DMF and DMTHF from HMF. A kinetic profile for the formation of these two molecules has been obtained, evidencing the existence of reaction intermediates on this catalytic system. The results of this study not only prove that monometallic Ni catalysts can lead to the selective hydroconversion of HMF to biofuel products, but also provide an understanding of the processes leading to the production both of DMF and DMTHF.

## Results and Discussion

### Catalyst characterization

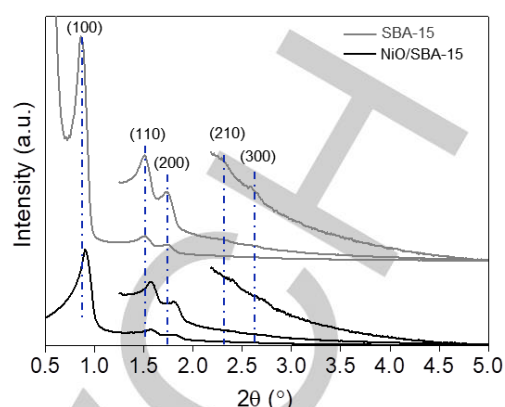


Figure 1. Low angle XRD patterns registered for SBA-15 and NiO/SBA-15.

Figure 1 depicts the low angle X-ray diffraction domain for NiO/SBA-15. Both the oxidized catalyst and the support exhibit one intense diffraction peak and four less intense diffraction peaks, indexed to the (100), (110), (200), (210) and (300) planes. It indicates that the ordered hexagonal 2D structure of *p6mm* symmetry in SBA-15 is well preserved after the formation of nickel oxide after calcination, as already reported [34]. The intensity decreases and the position shifts of the diffraction peaks of NiO/SBA-15 as compared to SBA-15 could be explained by the specific localization of the NiO NPs, mainly inside the support pores. Filling of pores reduces the electron density contrast between the pores and silica walls, affecting reflections positions and their intensities [34,35].

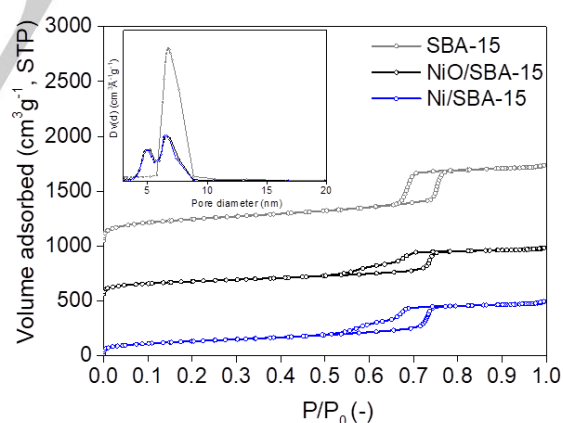


Figure 2. N<sub>2</sub> physisorption isotherms and BJH pore size distribution (inset) obtained for SBA-15, calcined NiO/SBA-15 and reduced Ni/SBA-15 catalyst (vertical shift of 500 cm<sup>3</sup>/g between isotherms for better clarity).

N<sub>2</sub> adsorption/desorption isotherms obtained for NiO/SBA-15 (calcined material) and Ni/SBA-15 (reduced material) are presented in Figure 2, and calculated textural properties are listed in Table 1. An isotherm shape of Type IV according to the IUPAC

classification is obtained for NiO/SBA-15, as obtained for the bare SBA-15 support. This confirms the retaining of a well ordered mesopore structure after the impregnation step and calcination. The change of the hysteresis shape, observed over the impregnated sample, with a two-step desorption and a delayed closure at lower relative pressure ( $P/P_0 = 0.46$  vs. 0.61 for the support) is indicative of the formation of NiO nanoparticles confined in the main mesopores of the SBA-15 [36,37]. Both open and NPs-filled cylindrical mesopores are expected to be present in the material. The B.J.H. pore size distribution (Figure 2 inset) shows consequently two maxima: a first maximum located at 6.6 nm, close to the diameter of the primary mesopores measured for the bare SBA-15 support; a second maximum located at 5.2 nm which is associated to the pores filled by the NiO particles. Both surface area and pore volume are observed to decrease after impregnation (>30% of decrease) which is coherent with the pore plugging phenomenon and the increase in material weight density after deposition. The further reduction step to obtain the Ni/SBA-15 catalyst does not induce significant change in either isotherm or hysteresis shapes. Only slight additional decreases in the surface area (-9%) and the pore volume (-6%) are observed while the pore size distribution remains almost unchanged, an evolution in part explained by the increase in material weight density with the formation of the metal phase.

The reducibility of NiO species was investigated by H<sub>2</sub>-TPR (Figure 3(A)). The H<sub>2</sub>-TPR profile of NiO/SBA-15 presents two main hydrogen consumption peaks, located at 389°C and 495°C, respectively, with a small H<sub>2</sub> consumption also visible at 300°C. According to the literature, the reduction of bulk NiO generally takes place at temperatures below 420°C [38,39]. Main hydrogen consumption (300 - 389°C) is then associated to NiO NPs behaving like bulk NiO: NiO NPs confined in the mesopores or large NiO particles located at the external surface of the silica grains. The consumption at 495°C, smaller, is associated to Ni species in stronger interaction with the silica support or to smaller size NiO NPs [40]. Quantification leads to a value of hydrogen consumed during the TPR experiment of 14.3 mmol/g. Such a value correspond to a >99% reduction degree of Ni(II) into Ni(0).

**Table 1.** Physico-chemical properties of SBA-15, NiO/SBA-15, Ni/SBA-15 and Ni/SBA-15-used (after reaction).

Catalyst	$S_{\text{BET}}$ , <sup>[a]</sup> m <sup>2</sup> /g	$V_t$ , <sup>[a]</sup> cm <sup>3</sup> /g	$D_p$ , <sup>[a]</sup> nm	$d_{\text{Ni}}$ , nm
SBA-15	841	1.10	6.8	-
NiO/SBA-15	519	0.70	5.2, 6.6	16.5 <sup>[b]</sup> , 15.9 <sup>[c]</sup>
Ni/SBA-15	468	0.66	5.2, 6.6	15.5 <sup>[b]</sup> , 14.7 <sup>[c]</sup>
Ni/SBA-15-used	242	0.50	4.9, 7.0	14.5 <sup>[b]</sup> , n.a. <sup>[d]</sup>

[a] B.E.T. surface area, total pore volume, and B.J.H. pore size obtained from N<sub>2</sub> physisorption; [b] Average crystal size measured for NiO or Ni using the Scherrer equation; [c] Average size measured from statistical analysis on TEM images. [d] n.a.: not analysed.

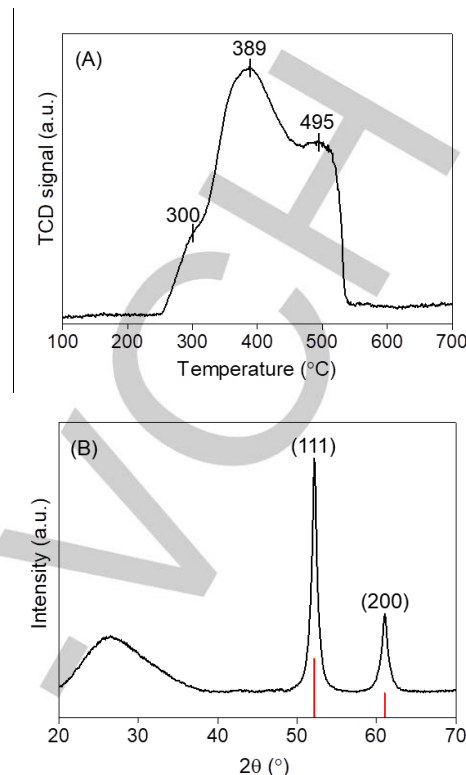


**Figure 3.** (A) H<sub>2</sub>-TPR profile for calcined NiO/SBA-15; (B) XRD pattern of reduced Ni/SBA-15 (vertical bars: JCPDS file n° 04-0850).

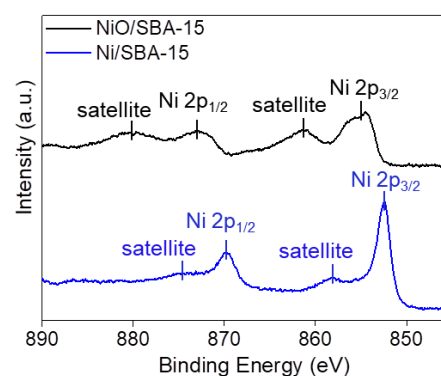


**Figure 4.** XPS high resolution spectra of Ni 2p core level obtained for NiO/SBA-15 and Ni/SBA-15 catalyst.

The speciation of nickel after reduction at 550°C for 2 h was first determined using XRD analysis (Figure 3(B)). Diffraction peaks at 52.2° and 61.0°, as well as the corresponding interplanar spacing values ( $d_{111} = 0.20$  nm,  $d_{200} = 0.18$  nm), indicate the presence of the cubic Ni(0) phase (JCPDS 04-0850). The shape of the diffraction peaks suggests the formation of both large and small Ni(0) crystals, with an average crystal domain size (calculated according to Scherrer equation) of 15.5 nm (Table 1). Spectra of Ni 2p core level were registered for NiO/SBA-15 and Ni/SBA-15

and are presented in Figure 4. Only Ni<sup>2+</sup> species (binding energy of 854.7 eV) are identified on the NiO/SBA-15 catalyst (calcined at 550°C) [41]. A significant evolution of the spectra was observed after reduction at 550°C: the Ni 2p<sub>3/2</sub> signal shifted to 852.5 eV, which indicates the formation of metallic Ni(0) [42], and the absence of residual oxidized nickel after treatment. TPR, XRD and XPS results then indicate the formation of purely metallic catalyst without remaining ionic nickel species, after a reduction performed at 550°C.

Dispersion of the nickel phase in the catalyst was further characterized by TEM (Figure 5). After activation of the catalyst under reducing conditions, the support always show a regular hexagonal arrangement of pores, in agreement with the conclusions issued from low angle XRD and N<sub>2</sub> physisorption. Besides, both empty and full mesopores exist in the structure. Two types of nickel particles are observed: as minor phase, large nickel particles (20-50 nm) (re)crystallized on the external surface of the silica grain (Figure 5A); as major phase, small oblong-shaped nickel NPs confined within the support channels, and having size of ~8 nm (width) - ~15 nm (length) (Figure 5B,C). As shown in the particle size distribution of the Ni NPs in Figure 5D, the size of most of the Ni particles were in the range of 5-15 nm, these particles being located within the main mesopores of the support. Notably, there exists a large population (14%) of external Ni particles (with a size larger than 20 nm).

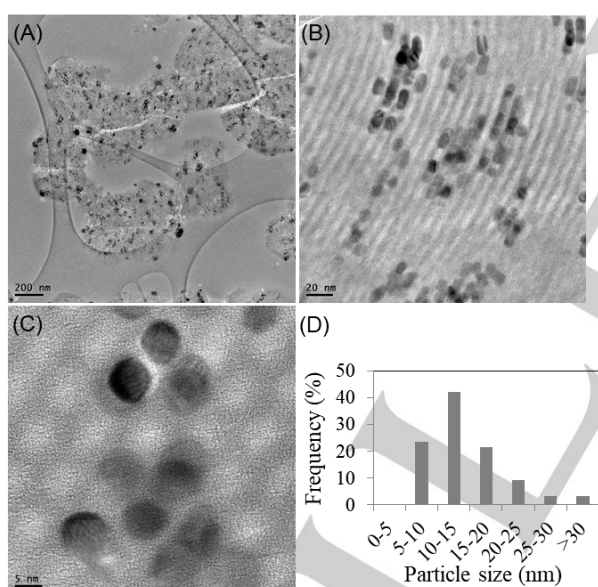


Figure 5. (A) Representative TEM images recorded for Ni/SBA-15; (B) Ni(0) particle size distribution obtained by statistical analysis of TEM images.

### Catalytic properties

In order to find the proper reaction parameters for high DMF/DMTHF yields over Ni/SBA-15, a set of orthogonal experiments were designed. Dioxane was chosen as the solvent, considering its stability in reaction, the solubility of HMF in this solvent and the better yields to target products than when other solvents are used [20]. The process parameters (i.e., reaction

temperature, H<sub>2</sub> pressure and HMF/Ni molar ratio) were selected on the basis of the available literature [43–45]. According to the literature, when the temperature is lower than 180°C, the hydrogenolysis of the C-O bond (the reaction affording the production of DMF/DMTHF) becomes slow [31]. 180°C was thus selected as the minimum temperature. The selectivity to DMF/DMTHF generally decreases with an increase of the reaction temperature above 240°C, owing to the formation of by-products such as humins [20,46]. Hence, the reaction temperature was set in the range of 180-240°C. The hydrogen pressure was chosen in the range 15-45 bar, considering that increasing hydrogen pressure increases the concentration of hydrogen in the solvent, which may benefit to the conversion rate. Maximum DMF/DMTHF yields were obtained below 50 bar [1]. Hence, 45 bar was selected as the maximum pressure level. Besides, the HMF/Ni molar ratio was varied in the range of 3-30, covering the range of the HMF/Ni molar ratios mentioned in the literature [1]. Once reaction parameters determined, a L<sub>9</sub> (3 (levels) ^ 3 (factors: T, P, HMF/Ni molar ratio)) orthogonal array was constructed according to the Taguchi method using software Minitab 17.

Table 2. Conversions and product distributions obtained under optimisation conditions<sup>[a]</sup>

No.	T /°C	P /bar	HMF/Ni mol. ratio	conv. /%	yield/%				C.B. /% <sup>[b]</sup>
					DMF	DMT HF	MFF R	MF OL	
1	180	15	30	7	1	0	1	2	97
2	180	30	3	100	1	81	1	1	85
3	180	45	15	34	12	0	2	10	90
4	210	15	3	100	1	72	1	1	76
5	210	30	15	44	41	1	2	0	100
6	210	45	30	21	17	1	1	2	100
7	240	15	15	32	21	3	8	0	100
8	240	30	30	11	7	1	1	2	100
9	240	45	3	100	0	55	1	1	58

[a] Catalytic tests were performed in batch-pressurized reactors, using a Autoplant-Chemspeed instrument, with 0.15 mmol/mL HMF in 25 mL 1,4-dioxane solution for 8 h. [b] carbon balance.

Reaction parameters, HMF conversion, main products yields and carbon balances are summarized in Table 2. Catalysis optimization results show that:

- (1) DMF, DMTHF, MFFR and MFOL were detected after 8 h of reaction in addition to DMTHF and DMF as the major products. These results indicate that the hydrogenolysis of C-OH bond and/or the furan ring hydrogenation are favored over the Ni/SBA-15 catalyst;
- (2) low HMF/Ni molar ratios ( $\leq 15$ ) or large catalyst quantity ( $\geq 0.052$  g) are required for efficient conversion of HMF;
- (3) hydrogen pressure in the selected range (15-45 bar) has a weaker influence on the catalytic results than the HMF/Ni molar ratio and the reaction temperature;
- (4) lower carbon balances (decreasing up to 58%) are obtained when HMF/Ni molar ratio decreases, an effect more visible at high

reaction temperatures (Table 2, Entry 4 and 9), due to possible polymerization reaction with BHMF and MFOL [43].

Two results out of the nine tests are worthy of noting. In Table 2 - Entry 5, a DMF yield of 40.6% at 43.8% HMF conversion was obtained at 210°C under 30 bar H<sub>2</sub> with a HMF/Ni molar ratio of 15, giving a maximum DMF selectivity (93%). However, the conversion of HMF is limited under these reaction conditions (low catalyst loading). In Table 2 - Entry 2, a DMTHF yield of 81.4% (100% HMF conversion) was obtained at 180 °C under 30 bar H<sub>2</sub> with a HMF/Ni molar ratio of 3, suggesting that these conditions are suitable for the selective production of DMTHF over Ni/SBA-15. This result is quite interesting considering that only one report in the literature reported similarly high DMTHF yield obtained with Ni-based catalysts [28]. Then, the high DMTHF yield obtained here suggests the possibility to optimize DMF yield under these reaction conditions according to the HMF → DMF → DMTHF pathway depicted in Scheme 1.

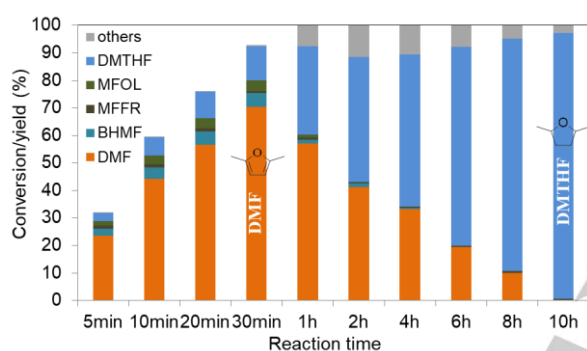


**Figure 6.** Evolution of HMF conversion and product yields with reaction time over Ni/SBA-15. Reaction conditions: 0.144 mmol/mL HMF in 25 mL 1,4-dioxane, P(H<sub>2</sub>) = 30 bar, T = 180°C, HMF/Ni molar ratio of 3.

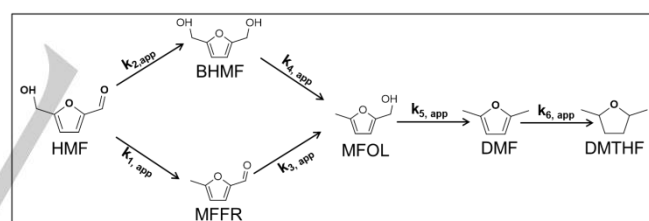
Evolution of HMF conversion and products yields with reaction time over Ni/SBA-15 (180°C, 30 bar H<sub>2</sub>, HMF/Ni molar ratio of 3) is depicted in Figure 6. It shows that at short reaction time (30 min), HMF was primarily converted into DMF (70.5% yield) in a fast way and the yield of DMTHF was limited (12.2% yield). BHMF and MFOL were also detected at low concentrations (4.9% and 4.0% yields, respectively). Almost no MFFR was detected (only 0.8% MFFR yield). BHMF could be converted into MFOL and DMF through the selective cleavage of the C-O bond (Scheme 1), the conversion of BHMF to MFOL followed by the hydrogenolysis of MFOL to DMF is consequently a possible route. The second route for DMF formation via MFFR and MFOL involves -CH<sub>2</sub>OH hydrogenolysis followed by -CHO hydrogenation, even if MFFR is measured at lower yield than BHMF. The DMF yield obtained after 30 min is quite comparable to the results obtained over monometallic Ni-based catalysts reported in the literature, especially considering that most catalytic performances previously reported rely on the use of functional supports (Table 3, Line 4-5). Results reported here then show that a simple monometallic Ni catalyst, even when supported over a neutral support, exhibits adequate surface properties affording fast

hydrogenolysis to selectively form DMF under optimized reaction conditions.

Prolonging the reaction time to 1 h leads to complete HMF conversion, with the conversion increase associated to a significant decrease of the DMF yield (57.0%) at the expense of the DMTHF yield (32.1%). The concentrations of BHMF and MFOL also decreased to negligible levels (yields <2%). During this period, the main reaction occurring is consequently the furan ring hydrogenation of DMF to produce DMTHF. When the reaction time is prolonged above 1 h, the yield of DMTHF continuously increased, reaching 96.6% at complete HMF conversion after 10 h. DMF yield is, after 10 h, at a negligible content (0.6%). Then, considering the evolution of intermediates and products yields with reaction time, HMF was rapidly converted into DMF via hydrogenolysis (BHMF and MFOL being main intermediates products identified). The furan ring hydrogenation of DMF to produce DMTHF is occurring at a slower rate, explaining the need of longer reaction time to maximize its yield. As compared to the reports available in the literature (Table 3, Entry 8-11), the DMTHF yield obtained in this work is among the highest reported. Only Kong et al. reported comparable result, with a bifunctional Ni-Al<sub>2</sub>O<sub>3</sub> catalyst (derived from the calcination of hydrotalcite-like precursor at high temperature, 850°C), with a comparable DMTHF yield (Table 3, Entry 11) after 20 h of reaction at 180°C under 12 bar and with a HMF/Ni molar ratio of 11 [28].

#### Kinetic of the reaction

A simplified kinetic model was defined (Scheme 2), lying on the hypotheses as described in the Supporting Information file.



**Scheme 2.** Kinetic scheme proposed for the DMTHF production from HMF ( $k_{app}$ : apparent rate constant)

The transformation of HMF to DMF and DMTHF supposes the formation of MFOL as intermediate (Scheme 2). Two hydrogenolysis steps take place sequentially, however, the hydrogenolysis of the aldehyde group requires an initial step of hydrogenation to -CH<sub>2</sub>OH [19]. MFOL itself can then be produced following two routes:

- (1) Hydrogenolysis of HMF to MFFR, followed by the hydrogenation of the aldehyde function of MFFR to MFOL.
- (2) Hydrogenation of the aldehyde function of HMF to BHMF, followed by the hydrogenolysis of BHMF to MFOL.

As DMTHF appears in the last stage, once DMF has been produced and accumulated, we suppose that the hydrogenation of the furan ring does not take place to a large extent on the minor intermediate products as BHMF and MFFR, and even MFOL [47]. When reaction is performed at 180°C, both MFFR and BHMF are

detected in small amounts at short reaction times. MFOL appears in parallel to BHMF, and not in a second stage as would be the case if it was produced only from BHMF. It is thus not possible to eliminate one of these two routes a priori.

Table 3. Catalytic performances of Ni-based catalysts for the conversion of HMF to DMF and DMTHF.

No.	Catalyst	Feed conditions	P (bar)	T (°C)	t (h)	X (%)	Y (%)	ref
<b>HMF to DMF</b>								
1	Raney Ni	12 mmol HMF; 35 mL 1,4-dioxane; 0.5 g catalyst	15	180	15	100	89	[31]
2	Ni/Ni <sup>2+</sup> -silicate <sup>[a]</sup>	12 mmol HMF; 38 mL 1,4-dioxane; 0.08 g catalyst	15	130	3	100	73	[32]
3	Ni/CN <sup>[b]</sup>	2 mmol HMF; 20 mL water; 0.05 g catalyst	30	200	6	100	99	[30]
4	Ni/LaFeO <sub>3</sub>	1 mmol HMF; 12 mL ethanol; 0.1 g catalyst	50	230	6	99	98	[27]
5	Ni/C	8 mmol HMF; 100 mL 1-propanol; W/F = 2 g.min/mL	33	180	-	92	53	[29]
6	Ni/Al <sub>2</sub> O <sub>3</sub>	12 mmol HMF, 35 mL 1,4-dioxane, 0.1 g catalyst	12	180	4	100	92	[28]
7	Ni/SBA-15	1.8 mmol HMF; 12.5 mL 1,4-dioxane; 0.261 g catalyst	30	180	0.5	93	71	<b>this work</b>
<b>HMF to DMTHF</b>								
8	Pd/C	8 mmol HMF, 100 mL 1-propanol	33	180	-	100	55	[29]
9	CuZn	4 mmol HMF, 20 mL CPME, 0.1 g catalyst	20	220	6	100	25	[17]
10	Ni/SiO <sub>2</sub>	12 mmol HMF, 38 mL 1,4-dioxane, 0.08 g catalyst	15	150	3	100	26	[32]
11	Ni/Al <sub>2</sub> O <sub>3</sub>	12 mmol HMF, 35 mL 1,4-dioxane, 0.1 g catalyst	12	180	20	100	97	[28]
12	Ni/SBA-15	1.8 mmol HMF; 12.5 mL 1,4-dioxane; 0.261 g catalyst	30	180	10	100	97	<b>this work</b>

[a] Ni(0)/Ni(II) catalyst from nickel phyllosilicate; [b]: Ni/CN, Ni supported on mesoporous nitrogen-rich carbon.

A fitting of the kinetic curve was performed by least-square minimization, according to the following steps [47,48]:

- HMF consumption was fitted using a first-rate law of rate constant ( $k_{1,app} + k_{2,app}$ ):

$$[HMF] = [HMF]_0 \exp(-(k_{1,app} + k_{2,app})t) \quad (1)$$

- As a primary intermediate product, MFFR neat production rate was defined as the difference between the production rate  $k_{1,app}$  [HMF] (HMF being consumed by paths 1 and 2) and the consumption rate  $k_{3,app}$  [MFFR], leading to Eq. (2):

$$[MFFR] = \frac{k_{1,app}[HMF]_0}{k_{3,app} - (k_{1,app} + k_{2,app})} [\exp(-(k_{1,app} + k_{2,app})t) - \exp(-k_{3,app}t)] \quad (2)$$

- As a primary intermediate product, BHMF neat production rate was defined as the difference between the production rate  $k_{2,app}$  [HMF] and the consumption rate  $k_{4,app}$  [BHMF], leading to Eq. (3):

$$[BHMF] = \frac{k_{2,app}[HMF]_0}{k_{4,app} - (k_{1,app} + k_{2,app})} [\exp(-(k_{1,app} + k_{2,app})t) - \exp(-k_{4,app}t)] \quad (3)$$

A first fitting of HMF consumption, and of MFFR and BHMF neat productions, led to the determination of the four first apparent rate constants,  $k_{1,app}$  to  $k_{4,app}$ , and to the calculation of  $r_1$  to  $r_4$ . It appeared that  $r_1$  is approximately 10 times higher than  $r_2$ , and that  $r_3$  was larger than  $r_4$  by a factor of 20 to 40. The main production path to MFOL was thus identified as the one involving MFFR (Scheme 3).

- The neat production of the secondary intermediate, MFOL, was then based on the HMF → MFFR → MFOL pathway, of rate constants  $k_{1,app}$  and  $k_{3,app}$ , for the production rate, and  $k_{5,app}$  for the consumption rate (Eq. 4):

$$[MFOL] = (k_{1,app} k_{3,app}) [HMF]_0 \left[ \frac{\exp(-k_{1,app}t)}{(k_{3,app} - k_{1,app})(k_{5,app} - k_{1,app})} - \frac{\exp(-k_{3,app}t)}{(k_{1,app} - k_{3,app})(k_{5,app} - k_{3,app})} + \frac{\exp(-k_{5,app}t)}{(k_{1,app} - k_{5,app})(k_{3,app} - k_{5,app})} \right] \quad (4)$$

allowing the fitting of constant  $k_{5,app}$  along with  $k_{1,app} - k_{4,app}$ .

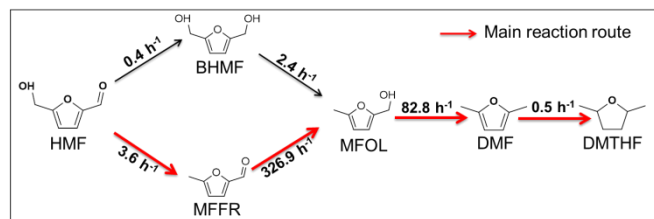
- As DMF is not the final product of reaction, it is not possible to model its production just by subtracting the concentrations of HMF, BHMF, MFFR and MFOL from  $[HMF]_0$ . However, BHMF, MFFR and MFOL being formed in very low amounts with respect to DMF and DMTHF, it can be attempted to apply the steady state approximation to these intermediates, and consider that the production rate of DMF is close to the consumption rate of HMF. DMF thus becomes an intermediate between HMF and DMTHF, and its concentration follows the law:

$$[DMF] = \frac{(k_{1,app} + k_{2,app})[HMF]_0}{k_{6,app} - (k_{1,app} + k_{2,app})} [\exp(-(k_{1,app} + k_{2,app})t) - \exp(-k_{6,app}t)] \quad (5)$$

making it possible to fit  $k_{6,app}$  with the other constants.

(6) Finally, DMTHF is calculated as the difference between  $[HMF]_0$ , and the concentrations of all the other products, including the unknown ones (implicitly supposing that they derive from the last stages of the global reaction).

After least-square minimization, the values of the six apparent reaction constants are determined as presented in Scheme 3.



**Scheme 3.** Apparent rate constants for each reaction step of HMF conversion to DMTHF

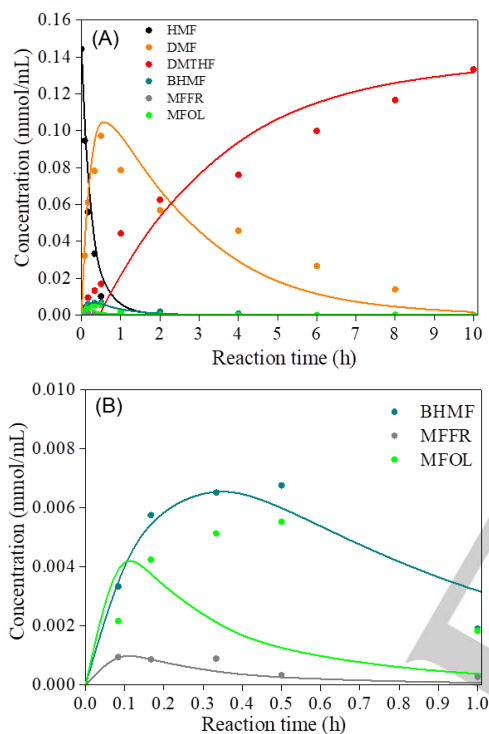


**Figure 7.** Kinetic patterns of HMF conversion over Ni/SBA-15 simulated using KaleidaGraph software (A), the enlargement of the kinetic patterns during the first hour (B). Reaction conditions: 0.144 mmol/mL HMF in 12.5 mL 1,4-dioxane,  $P(\text{H}_2) = 30$  bar,  $T = 180^\circ\text{C}$ , HMF/Ni molar ratio of 3, data points and solid lines represent experimental data and model, respectively.

A graphical comparison between the experimental and the modelled concentrations (Figure 7) raises the following comments: (1) HMF consumption, MFFR production and BHMf production are correctly modelled, in particular the position of the maximum of production of MFFR and BHMf. (2) In contrast, the production of MFOL is poorly reproduced, as its consumption starts too early. Decreasing  $k_{5,\text{app}}$  shifts the maximum of production to longer times, but also increases considerably the amount of MFOL formed, which means that  $k_{3,\text{app}}$  would also need to be better adjusted. There is thus a certain uncertainty on the values of  $k_{3,\text{app}}$  and  $k_{5,\text{app}}$  obtained by this model. A new fitting based only on the concentrations of the minor species led to a decrease of the two rate constants, but at the

expense of the quality of the fitting for BHMf. In any case,  $k_{3,\text{app}}$  and  $k_{5,\text{app}}$  were still large compared to  $k_{2,\text{app}}$  and  $k_{4,\text{app}}$ .

(3) The fits for DMF and DMTHF follow the same tendency as the experimental data, though at longer times the consumption of DMF and the production of DMTHF are overestimated. Some inhibition phenomena not taken into account in this simplified model can be postulated.

In summary, this simplified model shows that both C=O hydrogenation and hydrogenolysis steps are fast compared to the hydrogenation of the furan ring. C-O hydrogenolysis and C=O hydrogenation reactions are in competition. The MFFR route seems to be predominant, confirming the capability of the Ni catalyst for the hydrogenolysis reaction. The apparent rate constants of the hydrogenation and hydrogenolysis steps involving intermediates containing a methyl group (MFFR, MFOL) are found to be much larger than the others steps, suggesting a fast adsorption/reaction of these molecules on the catalyst surface. However, uncertainties remain large concerning the intermediates detected in low amounts.

### Stability of Ni/SBA-15

Recyclability of the SBA-15 supported Ni catalyst was evaluated (Figure 8). Between each reaction cycle, the catalyst was recovered by centrifugation after the reaction followed by washing with acetone. Then the catalyst was re-calcined at  $500^\circ\text{C}$  for 6 h and re-reduced at  $550^\circ\text{C}$  for 2 h before the next test. Each test was performed for 3 h at  $180^\circ\text{C}$  under 30 bar  $\text{H}_2$ . HMF conversion was 100% with the DMF yield of 45% and DMTHF yield of 48% in the first run (Figure 8). After 3 cycles of catalysis, HMF conversion decreased to 75% while the DMF yield and DMTHF yield reduced to 37% and 10%, respectively. This evolution indicated that the catalyst progressively deactivated during the tests.

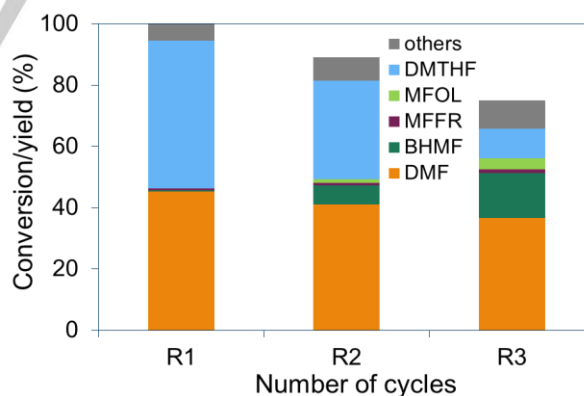


**Figure 8.** Recyclability of the Ni/SBA-15 catalyst for the HMF hydrogenation reaction. Reaction conditions: 0.15 mmol/mL HMF in 20 mL 1,4-dioxane,  $P(\text{H}_2) = 30$  bar,  $T = 180^\circ\text{C}$ , HMF/Ni molar ratio of 3, 3 h.

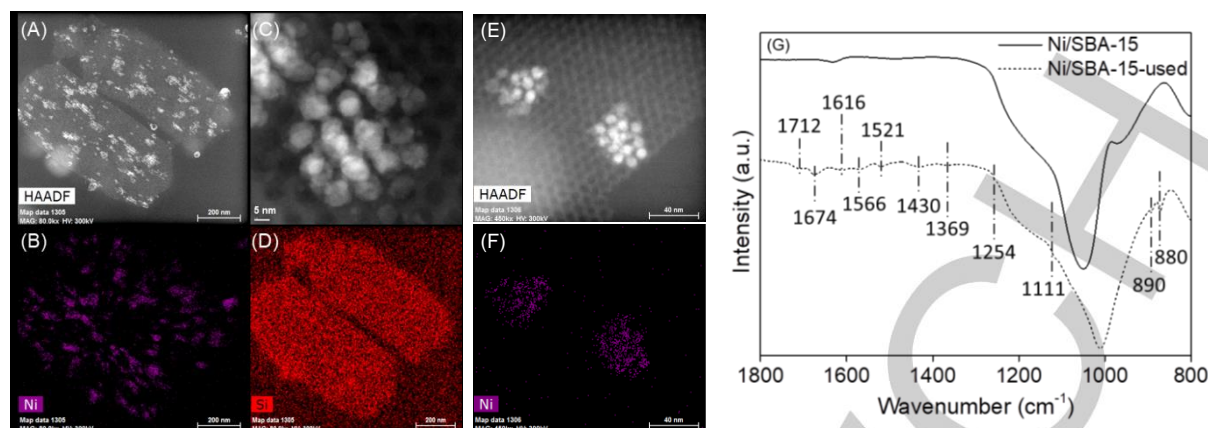


**Figure 9.** HAADF image (A,C,E) and Ni (B,F) and Si (D) mapping of the Ni/SBA-15-used sample; (G) FT-IR spectra of the fresh and used Ni/SBA-15 catalyst.

After the reaction, the spent catalyst was analysed by different characterization techniques in order to identify the main reason of the catalyst deactivation. As a first result, no evident growth of Ni crystal size was measured, applying the Scherrer equation to the XRD pattern recorded to the Ni/SBA-15-used catalyst (Table 1). The absence of significant sintering during reaction was confirmed by microscopy analysis results (Figure 9A-F), with no visible degradation of the mesostructured quality. Indeed, the majority of the particles are confined in well-defined mesopores of SBA-15 support, with a few aggregated Ni particles outside the channels (Figure 9A,B). Consequently, the deactivation is not associated to modifications of the support characteristics or Ni phase dispersion. Another possible way of deactivation is the adsorption of high molecular weight products on the active sites during the reaction [49]. The FT-IR spectra, shown in Figure 9E for the used catalyst, exhibits visible bands at:

- 880 cm<sup>-1</sup> (adsorption of furan compounds [50,51])
- 890 and 1254 cm<sup>-1</sup> (vibrations involving the C-H groups [52])
- 1111, 1369 and 1430 cm<sup>-1</sup> (C-O stretching vibration [53])
- 1521, 1566, 1616, 1674 and 1712 cm<sup>-1</sup> (assigned to C=O groups [53])

These results, added to the results obtained by TG-DSC and demonstrating a 2.3 wt.% carbon loss during temperature programmed oxidation up to 900 °C, indicate that the adsorption of organic intermediates on the catalyst surface [54] can be a reason of the progressive deactivation during recycling tests.

## Conclusions

Ni/SBA-15, prepared by the incipient wetness impregnation of nitrate precursor, is an active catalyst for the selective hydroconversion of 5-hydroxymethylfurfural (HMF) to 2,5-dimethylfuran (DMF) and 2,5-dimethyltetrahydrofuran (DMTHF). The existence of a large population of mesopore-confined NiO particles leads to a high reactivity. High yields of DMF and DMTHF are achieved, 70.5% and 96.6% respectively, by simply modifying the reaction time under optimized reaction conditions (180 °C, 30 bar). The catalyst exhibits a fast hydrogenolysis ability

and a high ability for the furan ring hydrogenation. The kinetic study demonstrated that HMF was probably converted via the route involving MFFR as an intermediate product. The competitive reactions, i.e. C-O hydrogenolysis and C=O hydrogenation, are fast as compared to the furan ring hydrogenation that is the reason of the possibility to reach high DMF yields. Further studies are however needed in order to improve the catalyst stability since 25% of the activity is lost after three reaction cycles, a deactivation preferably associated to carbon deposition on active element than to Ni nanoparticles sintering.

## Experimental Section

### Synthesis of Ni/SBA-15 catalyst

SBA-15 support was synthesized according to classical procedure [55]. In a typical synthesis, 4.0 g of Pluronic P123 was dissolved in a 1.6 M solution of HCl at 40 °C. Thereafter, 8.5 g of TEOS was added dropwise to the solution, and the solution was submitted to magnetic stirring for 24 h. The resulting gel was submitted for 48 h to hydrothermal ageing at 100 °C. After recovery by filtration, the SBA-15 sample was washed with water, and dried at 100 °C for 24 h. The dried SBA-15 sample was calcined at 550 °C for 6 h in a muffle furnace, using a heating ramp of 1.5 °C min<sup>-1</sup>.

The nickel catalyst was prepared using the incipient wetness impregnation – mild drying method (IWI-MD) [34]. To prepare 10 g of 15 wt.% Ni/SBA-15 catalyst, 9.4 mL of an aqueous solution of nickel nitrate (2.8 mmol/mL; Ni(NO<sub>3</sub>)<sub>2</sub>·6H<sub>2</sub>O, 98% purity, Sigma-Aldrich) was dropped into 8.5 g of SBA-15 powder (pore volume = 1.1 mL/g). The wet mixture was placed in an oven set at 25 °C and aged under static conditions for five days. A calcination under static air was finally performed at 500 °C for 6 h with a ramp of 1.5 °C/min. The calcined sample is denoted NiO/SBA-15, the reduced sample is denoted Ni/SBA-15 and the spent catalyst is denoted Ni/SBA-15-used.

### Characterization

X-ray diffraction patterns were recorded on a Bruker D8 Advance X-ray diffractometer in Bragg-Brentano configuration, with a Cu K $\alpha$  radiation ( $\lambda$  = 1.54184 Å). N<sub>2</sub> physisorption experiments were performed at -196 °C,

on a Micromeritics Tristar II Plus instrument. The particle size and shape were analysed by transmission electron microscopy. For fresh catalysts, experiments were conducted on a JEOL 2100 UHR, operated at 200 kV with a LaB<sub>6</sub> source and equipped with a Gatan 832 CCD camera. For the used catalyst, experiment was conducted on a TITAN Themis 300 S/TEM. The high angle annular dark field (HAADF) images were collected at angles between 50 and 200 mrad. H<sub>2</sub>-temperature programmed reduction (TPR) was performed on an Autochem analyzer (Micromeritics) equipped with a quartz U-shaped microreactor. Quantification of H<sub>2</sub> consumed is performed using a TCD after trapping of the produced water. The FT-IR spectra was registered on an infrared spectrometer with total attenuation (IR-ATR) from Thermo Scientific (IS50). Thermogravimetry experiments were conducted on a system from Mettler Toledo (TGA/SDTA 851 model). Experiment was conducted under 20%O<sub>2</sub> in N<sub>2</sub> flow at the rate of 50 mL/min, with temperature increase from 50°C to 900°C at an increase rate of 5 °C/min.

### Hydroconversion of 5-Hydroxymethylfurfural

Preliminary catalysis tests were performed in an 8-parallel automated autoclave system equipped with 8 high-pressure batch reactors (100 mL). Prior to the catalytic tests, the catalysts were reduced at 550 °C for 2 h (heating ramp of 10 °C/min) under 5 Vol.% H<sub>2</sub> in Ar flow (50 mL/min). Prior to the reaction, the reactor was charged under inert atmosphere (glove box) with 0.15 mmol/mL HMF in 25 mL 1,4-dioxane as a solvent and 0.16 g of catalyst, sealed and purged with H<sub>2</sub>. Then, the reactor was pressurized with required H<sub>2</sub> pressure (15–45 bar), heated at required temperature (180–240 °C) and stirred at a speed of 700 rpm for different reaction time. The kinetic profiles were performed in a 45 mL Parr reactor: the pre-reduced catalyst (550°C, 2 h, pure H<sub>2</sub> flow) was inserted in the reactor together with 12.5 mL of 0.15 mmol/mL HMF solution in 1,4-dioxane. The reactor was closed, purged with hydrogen gas for several times, and then pressurized with H<sub>2</sub> to obtain 30 bar of H<sub>2</sub> under the reaction conditions (T = 180 °C). The pressure was monitored using a gauge connected to the reactor. The reaction was stirred by magnetic agitation. Samples of reaction medium were taken off at selected reaction times: 5 min, 10 min, 20 min, 30 min, 1 h, 2 h, 4 h, 6 h, 8 h and 10 h. At the end of the reaction, the autoclave was rapidly cooled, and the catalyst was recovered by filtration. The products were analyzed by GC (Shimadzu 2010 Plus) equipped with ZB-WAX Plus capillary column (30.0 m × 0.25 mm × 0.25 μm) and a flame ionization detector (FID), and by GC-MS (Shimadzu QP2010 Ultra EI) equipped with a ZB-1XT capillary column (15.0 m × 0.53 mm × 0.25 μm) and a FID detector.

### Acknowledgements

Chevreul institute (FR 2638), Ministère de l'Enseignement Supérieur et de la Recherche and Région Hauts-de-France are also acknowledged for supporting this work. The authors thank Martine Trentesaux and Pardis Simon for XPS analysis, Olivier Gardoll for physical and redox characterization, Laurence Burylo for XRD experiment, Maya Marinova for TEM analysis and Svetlana Heyte from the REALCAT platform for high throughput catalytic tests.

**Keywords:** HMF • hydroconversion • nickel • biofuels • incipient wetness impregnation

[1] S. Chen, R. Wojcieszak, F. Dumeignil, E. Marceau, S. Royer, How Catalysts and Experimental Conditions Determine the Selective

- Hydroconversion of Furfural and 5-Hydroxymethylfurfural, *Chem. Rev.* 118 (2018) 11023–11117. doi:10.1021/acs.chemrev.8b00134.
- [2] R.-J. van Putten, J.C. van der Waal, E. de Jong, C.B. Rasrendra, H.J. Heeres, J.G. de Vries, Hydroxymethylfurfural, a versatile platform chemical made from renewable resources, *Chem. Rev.* 113 (2013) 1499–1597. doi:10.1021/cr300182k.
- [3] P. Gallezot, Conversion of biomass to selected chemical products, *Chem. Soc. Rev.* 41 (2012) 1538–1558. doi:10.1039/C1CS15147A.
- [4] J.-P. Lange, E. van der Heide, J. van Buijtenen, R. Price, Furfural-A Promising Platform for Lignocellulosic Biofuels, *ChemSusChem.* 5 (2012) 150–166. doi:10.1002/cssc.201100648.
- [5] K.J. Zeitsch, *The Chemistry and Technology of Furfural and its Many By-Products*, Elsevier, 2000.
- [6] G. Dautzenberg, M. Gerhardt, B. Kamm, Bio based fuels and fuel additives from lignocellulose feedstock via the production of levulinic acid and furfural, *Holzforschung.* 65 (2011) 439–451. doi:10.1515/hf.2011.081.
- [7] T.S. Hansen, K. Barta, P.T. Anastas, P.C. Ford, A. Riisager, One-pot reduction of 5-hydroxymethylfurfural via hydrogen transfer from supercritical methanol, *Green Chem.* 14 (2012) 2457–2461. doi:10.1039/C2GC35667H.
- [8] Y. Román-Leshkov, C.J. Barrett, Z.Y. Liu, J.A. Dumesic, Production of dimethylfuran for liquid fuels from biomass-derived carbohydrates, *Nature.* 447 (2007) 982–985. doi:10.1038/nature05923.
- [9] M.A. Jackson, M. Appell, J.A. Blackburn, Hydrodeoxygenation of Fructose to 2,5-Dimethyltetrahydrofuran Using a Sulfur Poisoned Pt/C Catalyst, *Ind. Eng. Chem. Res.* 54 (2015) 7059–7066. doi:10.1021/acs.iecr.5b00766.
- [10] J. Luo, H. Yun, A.V. Mironenko, K. Goulas, J.D. Lee, M. Monai, C. Wang, V. Vorotnikov, C.B. Murray, D.G. Vlachos, P. Fornasiero, R.J. Gorte, Mechanisms for High Selectivity in the Hydrodeoxygenation of 5-Hydroxymethylfurfural over PtCo Nanocrystals, *ACS Catal.* (2016) 4095–4104. doi:10.1021/acs.catal.6b00750.
- [11] L. Hu, X. Tang, J. Xu, Z. Wu, L. Lin, S. Liu, Selective Transformation of 5-Hydroxymethylfurfural into the Liquid Fuel 2,5-Dimethylfuran over Carbon-Supported Ruthenium, *Ind. Eng. Chem. Res.* 53 (2014) 3056–3064. doi:10.1021/ie404441a.
- [12] Q. Li, P. Man, L. Yuan, P. Zhang, Y. Li, S. Ai, Ruthenium supported on CoFe layered double oxide for selective hydrogenation of 5-hydroxymethylfurfural, *Molecular Catalysis.* 431 (2017) 32–38. doi:10.1016/j.mcat.2017.01.011.
- [13] S. Nishimura, N. Ikeda, K. Ebitani, Selective hydrogenation of biomass-derived 5-hydroxymethylfurfural (HMF) to 2,5-dimethylfuran (DMF) under atmospheric hydrogen pressure over carbon supported PdAu bimetallic catalyst, *Catalysis Today.* 232 (2014) 89–98. doi:10.1016/j.cattod.2013.10.012.
- [14] M. Chatterjee, T. Ishizaka, H. Kawanami, Hydrogenation of 5-hydroxymethylfurfural in supercritical carbon dioxide–water: a tunable approach to dimethylfuran selectivity, *Green Chem.* 16 (2014) 1543–1551. doi:10.1039/C3GC42145G.
- [15] J. Luo, J.D. Lee, H. Yun, C. Wang, M. Monai, C.B. Murray, P. Fornasiero, R.J. Gorte, Base metal-Pt alloys: A general route to high selectivity and stability in the production of biofuels from HMF, *Applied Catalysis B: Environmental.* 199 (2016) 439–446. doi:10.1016/j.apcatb.2016.06.051.
- [16] B. Chen, F. Li, Z. Huang, G. Yuan, Carbon-coated Cu-Co bimetallic nanoparticles as selective and recyclable catalysts for production of biofuel 2,5-dimethylfuran, *Applied Catalysis B: Environmental.* 200 (2017) 192–199. doi:10.1016/j.apcatb.2016.07.004.
- [17] G. Bottari, A.J. Kumalputri, K.K. Krawczyk, B.L. Feringa, H.J. Heeres, K. Barta, Copper–Zinc Alloy Nanopowder: A Robust Precious-Metal-Free Catalyst for the Conversion of 5-Hydroxymethylfurfural, *ChemSusChem.* 8 (2015) 1323–1327. doi:10.1002/cssc.201403453.
- [18] W. Guo, H. Liu, S. Zhang, H. Han, H. Liu, T. Jiang, B. Han, T. Wu, Efficient hydrogenolysis of 5-hydroxymethylfurfural to 2,5-dimethylfuran over a cobalt and copper bimetallic catalyst on N-graphene-modified Al<sub>2</sub>O<sub>3</sub>, *Green Chem.* (2016). doi:10.1039/C6GC02630C.
- [19] Y. Zhu, X. Kong, H. Zheng, G. Ding, Y. Zhu, Y.-W. Li, Efficient synthesis of 2,5-dihydroxymethylfuran and 2,5-dimethylfuran from 5-hydroxymethylfurfural using mineral-derived Cu catalysts as versatile catalysts, *Catal. Sci. Technol.* 5 (2015) 4208–4217. doi:10.1039/C5CY00700C.
- [20] B. Seemala, C.M. Cai, C.E. Wyman, P. Christopher, Support Induced Control of Surface Composition in Cu–Ni/TiO<sub>2</sub> Catalysts Enables High Yield Co-Conversion of HMF and Furfural to Methylated Furans, *ACS Catal.* (2017) 4070–4082. doi:10.1021/acscatal.7b01095.
- [21] S. Srivastava, G.C. Jadeja, J. Parikh, Synergism studies on alumina-supported copper-nickel catalysts towards furfural and 5-hydroxymethylfurfural hydrogenation, *Journal of Molecular Catalysis A:*

- Chemical. 426, Part A (2017) 244–256. doi:10.1016/j.molcata.2016.11.023.
- [22] A.J. Kumalapati, G. Bottari, P.M. Erne, H.J. Heeres, K. Barta, Tunable and Selective Conversion of 5-HMF to 2,5-Furandimethanol and 2,5-Dimethylfuran over Copper-Doped Porous Metal Oxides, *ChemSusChem*. 7 (2014) 2266–2275. doi:10.1002/cssc.201402095.
- [23] J. Luo, M. Monai, C. Wang, J.D. Lee, T. Duchoň, F. Dvořák, V. Matolín, C.B. Murray, P. Fornasiero, R.J. Gorte, Unraveling the surface state and composition of highly selective nanocrystalline Ni–Cu alloy catalysts for hydrodeoxygenation of HMF, *Catal. Sci. Technol.* 7 (2017) 1735–1743. doi:10.1039/C6CY02647H.
- [24] P. Yang, Q. Xia, X. Liu, Y. Wang, Catalytic transfer hydrogenation/hydrogenolysis of 5-hydroxymethylfurfural to 2,5-dimethylfuran over Ni-Co/C catalyst, *Fuel*. 187 (2017) 159–166. doi:10.1016/j.fuel.2016.09.026.
- [25] X. Kong, Y. Zhu, H. Zheng, Y. Zhu, Z. Fang, Inclusion of Zn into Metallic Ni Enables Selective and Effective Synthesis of 2,5-Dimethylfuran from Bioderived 5-Hydroxymethylfurfural, *ACS Sustainable Chem. Eng.* 5 (2017) 11280–11289. doi:10.1021/acssuschemeng.7b01813.
- [26] Y.-B. Huang, M.-Y. Chen, L. Yan, Q.-X. Guo, Y. Fu, Nickel-Tungsten Carbide Catalysts for the Production of 2,5-Dimethylfuran from Biomass-Derived Molecules, *ChemSusChem*. 7 (2014) 1068–1072. doi:10.1002/cssc.201301356.
- [27] M.-Y. Chen, C.-B. Chen, B. Zada, Y. Fu, Perovskite type oxide-supported Ni catalysts for the production of 2,5-dimethylfuran from biomass-derived 5-hydroxymethylfurfural, *Green Chem.* 18 (2016) 3858–3866. doi:10.1039/C6GC00432F.
- [28] X. Kong, R. Zheng, Y. Zhu, G. Ding, Y. Zhu, Y.-W. Li, Rational design of Ni-based catalysts derived from hydrotalcite for selective hydrogenation of 5-hydroxymethylfurfural, *Green Chem.* 17 (2015) 2504–2514. doi:10.1039/C5GC00062A.
- [29] J. Luo, L. Arroyo-Ramírez, J. Wei, H. Yun, C.B. Murray, R.J. Gorte, Comparison of HMF hydrodeoxygenation over different metal catalysts in a continuous flow reactor, *Applied Catalysis A: General*. 508 (2015) 86–93. doi:10.1016/j.apcata.2015.10.009.
- [30] R. Goyal, B. Sarkar, A. Bag, N. Siddiqui, D. Dumbre, N. Lucas, S.K. Bhargava, A. Bordoloi, Studies of synergy between metal–support interfaces and selective hydrogenation of HMF to DMF in water, *Journal of Catalysis*. 340 (2016) 248–260. doi:10.1016/j.jcat.2016.05.012.
- [31] X. Kong, Y. Zhu, H. Zheng, F. Dong, Y. Zhu, Y.-W. Li, Switchable synthesis of 2,5-dimethylfuran and 2,5-dihydroxymethyltetrahydrofuran from 5-hydroxymethylfurfural over Raney Ni catalyst, *RSC Adv.* 4 (2014) 60467–60472. doi:10.1039/C4RA09550B.
- [32] X. Kong, Y. Zhu, H. Zheng, X. Li, Y. Zhu, Y.-W. Li, Ni Nanoparticles Inlaid Nickel Phyllosilicate as a Metal–Acid Bifunctional Catalyst for Low-Temperature Hydrogenolysis Reactions, *ACS Catal.* 5 (2015) 5914–5920. doi:10.1021/acscatal.5b01080.
- [33] P. Yang, Q. Xia, X. Liu, Y. Wang, High-yield production of 2,5-dimethylfuran from 5-hydroxymethylfurfural over carbon supported Ni–Co bimetallic catalyst, *Journal of Energy Chemistry*. (n.d.). doi:10.1016/j.jechem.2016.08.008.
- [34] A. Ungureanu, B. Dragoi, A. Chiriac, S. Royer, D. Duprez, E. Dumitriu, Synthesis of highly thermostable copper-nickel nanoparticles confined in the channels of ordered mesoporous SBA-15 silica, *J. Mater. Chem.* 21 (2011) 12529–12541. doi:10.1039/C1JM10971E.
- [35] S. Chen, C. Ciotonea, A. Ungureanu, E. Dumitriu, C. Catrinescu, R. Wojcieszak, F. Dumeignil, S. Royer, Preparation of nickel (oxide) nanoparticles confined in the secondary pore network of mesoporous scaffolds using melt infiltration, *Catalysis Today*. 334 (2019) 48–58. doi:10.1016/j.cattod.2019.01.064.
- [36] J. P. Thielemann, F. Girgsdies, R. Schlögl, C. Hess, Pore structure and surface area of silica SBA-15: Influence of washing and scale-up, *Beilstein Journal of Nanotechnology*. 2 (2011) 110–8. doi:10.3762/bjnano.2.13.
- [37] P.V.D. Voort, P.I. Ravikovitch, K.P.D. Jong, A.V. Neimark, A.H. Janssen, M. Benjelloun, E.V. Bavel, P. Cool, B.M. Weckhuysen, E.F. Vansant, Plugged hexagonal templated silica: a unique micro- and mesoporous composite material with internal silica nanocapsules, *Chem. Commun.* 0 (2002) 1010–1011. doi:10.1039/B201424F.
- [38] S.D. Robertson, B.D. McNicol, J.H. De Baas, S.C. Kloet, J.W. Jenkins, Determination of reducibility and identification of alloying in copper-nickel-on-silica catalysts by temperature-programmed reduction, *Journal of Catalysis*. 37 (1975) 424–431. doi:10.1016/0021-9517(75)90179-7.
- [39] R. Brown, M.E. Cooper, D.A. Whan, Temperature programmed reduction of alumina-supported iron, cobalt and nickel bimetallic catalysts, *Applied Catalysis*. 3 (1982) 177–186. doi:10.1016/0166-9834(82)80090-0.
- [40] C. Louis, Z.X. Cheng, M. Che, Characterization of nickel/silica catalysts during impregnation and further thermal activation treatment leading to metal particles, *J. Phys. Chem.* 97 (1993) 5703–5712. doi:10.1021/j100123a040.
- [41] A.A. Lemonidou, M.A. Goula, I.A. Vasalos, Carbon dioxide reforming of methane over 5wt.% nickel calcium aluminate catalysts – effect of preparation method, *Catalysis Today*. 46 (1998) 175–183. doi:10.1016/S0920-5861(98)00339-3.
- [42] X.-P. Yu, W. Chu, N. Wang, F. Ma, Hydrogen Production by Ethanol Steam Reforming on NiCuMgAl Catalysts Derived from Hydrotalcite-Like Precursors, *Catal Lett.* 141 (2011) 1228–1236. doi:10.1007/s10562-011-0608-0.
- [43] Y. Nakagawa, M. Tamura, K. Tomishige, Catalytic Reduction of Biomass-Derived Furanic Compounds with Hydrogen, *ACS Catal.* 3 (2013) 2655–2668. doi:10.1021/cs400616p.
- [44] L. Hu, L. Lin, S. Liu, Chemoselective Hydrogenation of Biomass-Derived 5-Hydroxymethylfurfural into the Liquid Biofuel 2,5-Dimethylfuran, *Ind. Eng. Chem. Res.* 53 (2014) 9969–9978. doi:10.1021/ie5013807.
- [45] L. Hu, G. Zhao, W. Hao, X. Tang, Y. Sun, L. Lin, S. Liu, Catalytic conversion of biomass-derived carbohydrates into fuels and chemicals via furanic aldehydes, *RSC Adv.* 2 (2012) 11184–11206. doi:10.1039/C2RA21811A.
- [46] A.S. Naggure, N. Lucas, S.V. Chilukuri, Efficient Preparation of Liquid Fuel 2,5-Dimethylfuran from Biomass-Derived 5-Hydroxymethylfurfural over Ru–NaY Catalyst, *ACS Sustainable Chem. Eng.* 3 (2015) 2909–2916. doi:10.1021/acssuschemeng.5b00857.
- [47] A.B. Gawade, M.S. Tiwari, G.D. Yadav, Biobased Green Process: Selective Hydrogenation of 5-Hydroxymethylfurfural to 2,5-Dimethyl Furan under Mild Conditions Using Pd-Cs<sub>2</sub>5H<sub>0</sub>5PW<sub>12</sub>O<sub>40</sub>/K-10 Clay, *ACS Sustainable Chem. Eng.* 4 (2016) 4113–4123. doi:10.1021/acssuschemeng.6b00426.
- [48] Y. Liu, M.A. Mellmer, D.M. Alonso, J.A. Dumesic, Effects of Water on the Copper-Catalyzed Conversion of Hydroxymethylfurfural in Tetrahydrofuran, *ChemSusChem*. 8 (2015) 3983–3986. doi:10.1002/cssc.201501122.
- [49] J. Chen, F. Lu, J. Zhang, W. Yu, F. Wang, J. Gao, J. Xu, Immobilized Ru Clusters in Nanosized Mesoporous Zirconium Silica for the Aqueous Hydrogenation of Furan Derivatives at Room Temperature, *ChemCatChem*. 5 (2013) 2822–2826. doi:10.1002/cctc.201300316.
- [50] Y.-L. Liu, C.-Y. Hsieh, Crosslinked epoxy materials exhibiting thermal remendability and removability from multifunctional maleimide and furan compounds, *Journal of Polymer Science Part A: Polymer Chemistry*. 44 (2006) 905–913. doi:10.1002/pola.21184.
- [51] A. Gandini, D. Coelho, M. Gomes, B. Reis, A. Silvestre, Materials from renewable resources based on furan monomers and furan chemistry: work in progress, *J. Mater. Chem.* 19 (2009) 8656–8664. doi:10.1039/B909377J.
- [52] C. Moreno-castilla, F. Carrasco-marín, F.J. Maldonado-hódar, J. Rivera-utrilla, Effects of non-oxidant and oxidant acid treatments on the surface properties of an activated carbon with very low ash content, *Carbon*. 36 (1998) 145–151. doi:10.1016/S0008-6223(97)00171-1.
- [53] U.J. Kim, C.A. Furtado, X. Liu, G. Chen, P.C. Eklund, Raman and IR Spectroscopy of Chemically Processed Single-Walled Carbon Nanotubes, *J. Am. Chem. Soc.* 127 (2005) 15437–15445. doi:10.1021/ja052951o.
- [54] L. Yu, L. He, J. Chen, J. Zheng, L. Ye, H. Lin, Y. Yuan, Robust and Recyclable Nonprecious Bimetallic Nanoparticles on Carbon Nanotubes for the Hydrogenation and Hydrogenolysis of 5-Hydroxymethylfurfural, *ChemCatChem*. 7 (2015) 1701–1707. doi:10.1002/cctc.201500097.
- [55] D. Zhao, J. Feng, Q. Huo, N. Melosh, G.H. Fredrickson, B.F. Chmelka, G.D. Stucky, Triblock Copolymer Syntheses of Mesoporous Silica with Periodic 50 to 300 Angstrom Pores, *Science*. 279 (1998) 548–552. doi:10.1126/science.279.5350.548.

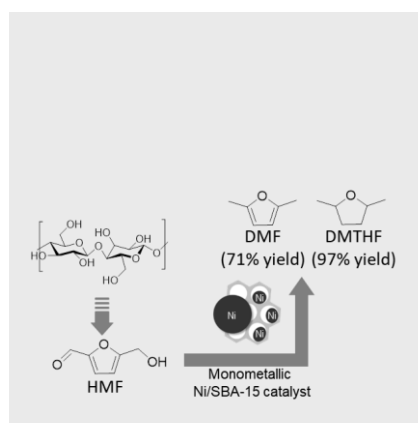
## FULL PAPER

## Entry for the Table of Contents (Please choose one layout)

Layout 1:

## FULL PAPER

Text for Table of Contents

*Author(s), Corresponding Author(s)\****Page No. – Page No.****Title**

Layout 2:

## FULL PAPER

((Insert TOC Graphic here; max. width: 11.5 cm; max. height: 2.5 cm))

*Author(s), Corresponding Author(s)\****Page No. – Page No.****Title**

Text for Table of Contents